Route planning for orchard operations

Published version:

DOI:10.1016/j.compag.2014.12.024

(Article begins on next page)

Route planning for orchard operations

D. Bochtis[1,*]; H.W. Griepentrog[2]; S. Vougioukas[3]; P. Busato[4]; R. Berruto; K. Zhou[1]

[1] Department of Engineering, University of Aarhus, Blichers Allé 20, 8830 Tjele, Denmark

[2]Institute of Agricultural Engineering, University of Hohenheim, 70599 Stuttgart, Germany

[3]Department of Biological and Agricultural Engineering, University of California, 95616 Davis, USA

[4] Dept. of agriculture, food and forestry sciences DISAFA, University of Turin, 10095, Grugliasco, Italy

[*] Corresponding author: Dionysis.Bochtis@eng.au.dk

Abstract

Orchard operations are considered a promising area for the implementation of robotic systems because of the inherent structured operational environment that arises from time-independent spatial tree configurations. In this paper, a route planning approach is developed and tested using a deterministic behaviour robot (named AMS - autonomous mechanisation system). The core of the planning method is the generation of routing plans for intra- and inter-row orchard operations, based on the adaptation of an optimal area coverage method developed for arable farming operations (B-patterns). Experiments have verified that operational efficiencies can be improved significantly compared with the conventional, non-optimised method of executing orchard operations. Specifically, the experimental results showed that the non-working time reduction ranged between 10.7% and 32.4% and that the reduction in the non-working distance ranged between 17.5% and 40.2% resulting to savings in the total travelled distance ranged between 2.2% and 6.4%.

Keywords: Operations management; autonomous vehicle; mission planning;

1. INTRODUCTION

Orchard operations are considered a promising area for the implementation of robotic systems because of the inherent structured operational environment that arises from time-independent spatial tree configurations. Trees have well-defined locations, and consequently, the inter- and intra-row distances are time-independent enough that route planning doesn't need to be performed every time the robot visits the block but only when its configuration changes. Based on these operational features of orchards, a number of dedicated robotic systems have been developed and prototyped. Selective examples include robots for cherry harvesting (Tanigaki et al., 2008) and apple harvesting (De-An et al., 2011). A number of navigation technologies for vehicles operating in orchards have been developed in parallel to these efforts; examples of early attempts include guidance systems based on cables (Tosaki et al., 1996), using physical contact sensors (Yekutieli and Pegna, 2002), using ultrasonic sensors combined with DGPS (Iida and Burks, 2002), and using machine vision and laser radar (Tsubota et al., 2004; Subramanian et al., 2006; Barawid Jr et al., 2007; Subramanian et al., 2009). Furthermore, navigation methods from row crop systems could be efficiently applied in orchards. These include machine vision, laser scanner, and stereovision approaches (Rovira-Mas et al., 2005; Kise et al., 2005; Hiremath et al., 2014a; Hiremath et al., 2014a). The aforementioned sensing technologies are considered an integrated part of the system combined with real time path planning modules for the case of robotic systems. These include methods that have been developed specifically for orchards (e.g., Linker and Blass, 2008) or general grid-based path planning approaches from research into off-road robotics (e.g., Ferguson and Stentz, 2006).

In this paper, a route planning approach for orchard operations is developed and tested using a deterministic behaviour robot. The core of the planning method is the generation of routing plans for intra- and inter-row orchard operations, based on the adaptation of an optimal area coverage method developed for arable farming operations (B-patterns).

2. MATERIALS AND METHODS

2.1 B-PATTERNS IN ARABLE FARMING

B-patterns were introduced by Bochtis (2008) and are defined as "*algorithmically-computed sequences of field-work tracks completely covering an area and that do not follow any pre-determined standard motif, but in contrast, are a result of an optimization process under one or more selected criteria*" (Bochtis et al, 2013). The aforementioned optimisation process of finding the optimal traversal sequence of the fieldwork tracks is based on finding the shortest tour (or tours, in the case of operations constrained by material carrying capacity of the machine) in an weighted graph. In the case presented here, the optimisation criterion minimises the total non-working travelled distance by the robotic vehicle while executing an orchard operation.

The general optimisation problem underlying the generation of B-patterns is finding the optimal permutation (Bochtis et al, 2013):

$$\sigma^* = \arg\min_{\sigma} \left[c_{0,p^{-1}(1)} + \sum_{i=1}^{|T|} c_{p^{-1}(i+1),p^{-1}(i)} + c_{p^{-1}(|T|),f} \right]$$

where $T = \{1,2,3,...\}$ is the ordered set of the field-work tracks that cover a field area (or equivalently, in the presented case, the tracks required for the complete execution of an orchard operation), $\sigma =< p^{-1}(1), p^{-1}(2),..., p^{-1}(|T|) >$ is a permutation (σ^* the optimal one) of the inverse function of the bijection $p(\cdot) : T \to T$, which for any track $i \in T$, returns its order in the track traversal sequence in which the agricultural vehicle executes the operation, $c_{0p^{-1}(1)}$ is the cost for the agricultural vehicle to move from the entry point (of the field or the orchard) to the first track in the traversal sequence, $c_{p^{-1}(|T|),f}$ is the cost for the vehicle to move from the end of the last track in the traversal sequence to the exit point, and $c_{p^{-1}(i+1),p^{-1}(i)}$ is the cost for moving between tracks $p^{-1}(i+1)$ and $p^{-1}(i)$. In this case, the cost corresponds to the non-working travelled distance for moving from one track to a subsequent one.

It has been proven that the B-patterns generation problem can be cast as a vehicle routing problem (VRP); consequently, any algorithmic procedure developed to solve the VRP can be employed in the B-patterns generation problem (*cf.* Bochtis and Sørensen (2009) for an extensive presentation of casting different types of field area operations to different instances of the VRP).

To generate the optimisation problem graph, the approach introduced by Bochtis et al. (2009) for mission planning on the same robotic platform was implemented in this work. In this approach, two nodes represent each track, one for each track ending. To implement a solver for the corresponding VRP, the matrix containing the connection cost between any nodes of the graph must be derived. Bochtis et al. (2009) showed that in the case of representation of a track using two nodes, this matrix is composed of $|T|^2$ inter-row 2×2 matrices and is given by

$$\mathrm{A} = \begin{bmatrix} \mathrm{O} & \mathrm{A}_{12} & \cdots & \mathrm{A}_{|T|n} \\ \mathrm{A}_{21} & \ddots & & \\ \vdots & & \ddots & \\ \mathrm{A}_{|T|1} & \cdots & \cdots & \mathrm{O} \end{bmatrix}$$

where O is the zero 2×2 matrix and A_{ij} is the a matrix that is defined by

$$\mathrm{A}_{ij} = \begin{bmatrix} c_{ij}^{u} & M \\ M & c_{ij}^{l} \end{bmatrix}, \quad i,j \in T$$

where M is a relatively (to the arc weight values in the problem) large number and is assigned as the cost for non-permitted connections and c_{ij}^{u}, c_{ij}^{l} are the costs for the connection between tracks i and j from the upper and lower headland, respectively. The cost that is assigned to a permitted connection of a pair of nodes represents the length of the shortest headland turn between the corresponding tracks to the nodes. In general, this length (in an obstacle-free space) is a function of the starting and ending points of the turn (i.e., on the same headland ending points of the tracks that are connected), the turning radius of the vehicle, and the direction of movement on the track from where the turn is initiated: $\Lambda(i,j) \mapsto P(x_i, y_i, x_j, y_j, r_{\min}, d)$. This can be produced, in principle, by implementing any path-planning algorithm. In the presented case, to calculate the lengths of these headland turns, the Dubins' Theorem and the Reeds-Shepp Theorem for non-holonomic systems have been implemented to geometrically define the most common headland turns of an Ackerman-steering based agricultural vehicle, i.e., the pi-turn (Π-turn), the omega-turn (Ω-turn), and the tau-turn (Tau-turn) (Bochtis and Vougioukas, 2008). In the simple case of rectangular fields, which is the case for the experimental orchards presented in this paper, the turning length is a function of the distance $s(i,j)$ between the two connected tracks $i, j \in T$ and the relation between this distance and the minimum turning radius of the vehicle. Specifically,

$$\Lambda(i,j) = \Lambda(s(i,j)) = \begin{cases} \mathrm{X}(s(i,j)), & s(i,j) < 2r_{\min}, \ \mathrm{X} \in \{\mathrm{Tau}, \Omega\} \\ \Pi(s(i,j)), & s(i,j) \geq 2r_{\min} \end{cases}$$

In the case of area coverage field operations, the distance $s(i,j)$ is a multiple of the machine's operating width, w, e.g., $s(i,j) = |i-j|w$. However, in the case of orchard operations, this does not hold true.

The goal of the next paragraphs is to determine how the function $s(i, j)$ is formulated for different types of orchard operations and how, based on this function, the cost matrix corresponding to the operation VRP is created.

It is worth noting that, depending on the orchard spatial configuration (i.e., number and length of rows, etc.), there are cases where to visit all tracks the robot might need to drive on some tracks more than once even without working there (e.g., the mower is lifted or the sprayer is turned off). In the presented approach, due to the VRP underlying methodology, it is assumed that each track is visited exactly once (when it is worked) and all interconnections (between rows and between a row and the entry-exit points of the orchard) take place by travelling on the headland area of the orchard.

2.2 MODELLING OF B-PATTERNS IN ORCHARD OPERATIONS

In the following, the term "track" refers to the trip that the machine travels while operating that starts at one end of the orchard and terminates at its opposite end, the term "row" refers to a cluster of trees to which the machine operates parallel, and the term "*corridor*" refers to the intra-row space. Two types of operations categorise orchard operations: inter-row operations (e.g., grass mowing in the corridors and spraying using a mist blower for pest control) and intra-row operations (e.g., mechanical weeding, spraying using nozzle sprayers).

2.2.1 Intra-Row Operations

During intra-row operations, the machine performs two trips per a row of trees (one trip for each side of the row, as shown in Figure 1). Consequently, if κ denotes the number of rows, the machine has to traverse a total of 2κ tracks ($|T| = 2\kappa$) to complete the operation.

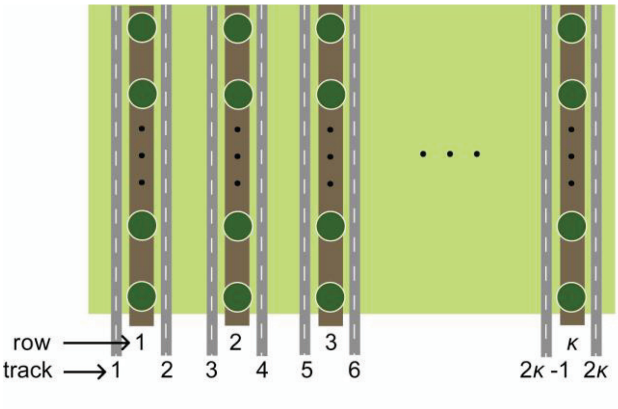

Figure 1. The derived tracks for intra-row orchard operations.

One of the orchard's headlands is arbitrarily called the "upper" headland, and the other is called the "lower" headland. The $2 \times \kappa$ matrix $\mathbf{U_R}$ is defined by the elements $u_R(1,i)$ and $u_R(2,i)$ where $i = 1,...,\kappa$. They represent the x- and y-coordinates, respectively, of the location of the last tree of row i on the upper headland. Similarly, a $2 \times \kappa$ matrix $\mathbf{L_R}$ is defined that corresponds to the lower headland. It should be noted that the above-mentioned matrices are inputs of the routing problem with elements (coordinates of trees) derived from GPS measurements. The $2 \times 2\kappa$ matrices $\mathbf{U_T}$ and $\mathbf{L_T}$ correspond to $\mathbf{U_R}$ and $\mathbf{L_R}$ and are defined with the x- and y-coordinates of the locations of the tracks' ends at the upper and lower headlands, respectively. The elements of $\mathbf{U_T}$ (and equivalently of the matrix $\mathbf{L_T}$) can be derived using the following expression:

$$u_T(n,i) = u_R\left(n, \frac{i + \mathrm{mod}(i,2)}{2}\right) + \mu(-1)^i \left[\mathrm{mod}(n,2)\sin\theta + \mathrm{mod}(n-1,2)\cos\theta\right]$$

where $i \in \{1,...2\kappa\}$, $n = \{1,2\}$, μ is the distance between the row in which the machine operates and the centre line of the transverse plane to the tractor (Figure 2), and θ is the inclination of the row line.

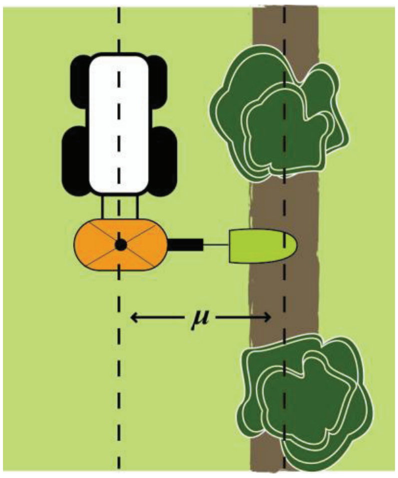

Figure 2. Vehicle positioning in intra-row operations

The distance between the two tracks *i* and *j* is thus:

$$s_u(i,j) = \left(\left(u_T(1,i) - u_T(1,j) \right)^2 + \left(u_T(2,i) - u_T(2,j) \right)^2 \right)^{\frac{1}{2}}$$

One-way oriented implements carry out intra-row operations. The specific placement of the implement does not allow for transitions between specific track sequences. For example, Figure 3a shows that if the machine (carrying the implement on its right side) is currently working while moving on track *j*, the next tracks on which it can move are tracks *j*-1, *j*+1, *j*+3,…, but it cannot move on tracks *j*-2, *j*+2,…. . In the latter case, the implement and the row to be worked would be bilaterally located to the machine (Figure 3b). In general, the allowed transitions between tracks are either from tracks of even parity to tracks of odd parity, or the opposite. In contrast, transitions between tracks of identical parity are not allowed. Consequently, the transition between tracks *i* and *j* is allowed only if the condition $\mathrm{mod}(|i-j|,2) = 1$ holds true.

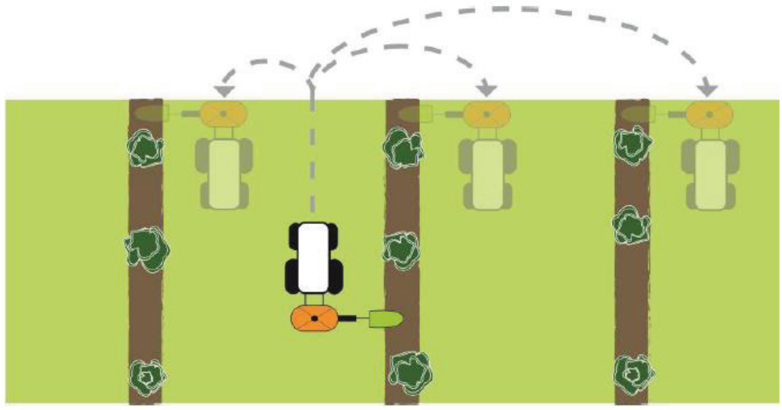

(a)

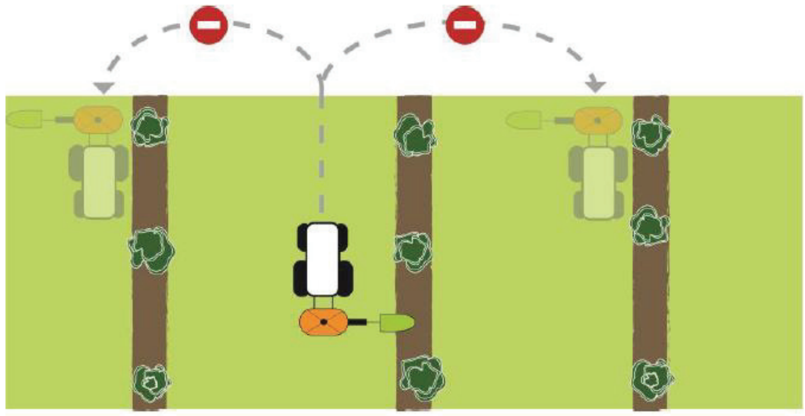

(b)

Figure 3 – Disallowed transitions for a robot carrying a one-way oriented implement.

Based on that, the elements of the matrix $\mathbf{A}_{ij}$ can be written as

$$c_{ij}^{u} = \Lambda\left(s^{u}(i,j)\right)\cdot \mathrm{mod}(|i-j|,2) + \mathrm{mod}(1+|i-j|,2)\cdot M$$

When i and j are of identical parity, the term $\mathrm{mod}(1+|i-j|,2)$ equals 1, and the term $\mathrm{mod}(|i-j|,2)$ equals 0. Consequently, the transition cost is equivalent to *M,* whereas in the opposite case, the values of the previous terms are reversed and the matrix element corresponds with the actual distance for turning between the two tracks.

2.2.2 Inter-Row Orchard operations

For simplicity reasons, the presentation of the method is limited to the case in which the inter-row distances between any pair of adjacent rows are identical. Modelling inter-row operations can be considered an extension of B-patterns implementation in numerous sub-fields (or neighbouring fields) (Bochtis and Vougioukas, 2008). Following this approach, each corridor can be considered a distinctive sub-area of the total area that must be covered.

Let *v* denote the number of field work tracks required for covering an internal corridor area. The number of distinctive (virtual) fields is equal to κ+1, where κ-1 fields correspond to corridors and the other two boundary fields correspond to the outer parts of the first and last tree rows. Let T_1 and $T_{\kappa+1}$ denote the track sets of the boundary sub-field areas of the orchard, and let $T_i,\ i=2,\ldots,\kappa$ denote the track sets of the field corresponding to the κ-1 orchard corridors (in which $|T_2|=|T_3|=\ldots=|T_\kappa|=\nu$). The union of all tracks provides the track set of the field that corresponds to the total orchard area that must be worked:

$$T=\Delta_1\cup\Delta_2\cup\ldots\cup\Delta_{\kappa+1}$$

where

$$\Delta_i=\left\{\sum_{j=1}^{i-1}|T_j|+1,\sum_{j=1}^{i-1}|T_j|+2,\ldots,\sum_{n=j}^{i-1}|T_j|+|T_j|\right\},\ \ i=1,\ldots,\kappa+1$$

Considering a "virtual" tree row indexed as row "0", a sub-field corresponds to each tree row (e.g., the 0 row corresponds to sub-field 1). For any element *i* of set *T*, the number of the tree row $\delta(i)$ to which track *i* belongs can be conversely derived using the following function:

$$\delta(i)=\left\lfloor\frac{i-1-|T_1|}{\nu}\right\rfloor+1$$

The distance $D_{a\to b}$ between the corresponding tree rows *a* and *b* to which tracks *i* and *j* belong is given by

$$D^{u}_{a\to b} = D^{u}_{\delta(i)\to\delta(j)} = \begin{cases} \left(\left(u_R(1,\delta(i)) - u_R(1,\delta(j))\right)^2 + \left(u_R(2,\delta(i)) - u_R(2,\delta(j))\right)^2\right)^{\frac{1}{2}}, \delta(i),\delta(j) \neq 0 \\ D^{u}_{\delta(1)\to\delta(j)} + \mu + w\left(\left|T_1\right| - 1\right), \quad \delta(i) = 0, \delta(j) \neq 0 \\ 0, \quad \delta(i) = 0, \delta(j) = 0 \end{cases}$$

The relative position of track *i* in the specific sub-field is given by

$$i^{*} = \begin{cases} i & i \leq \left|T_1\right| \\ i - \left[\left(\delta(i) - 1\right)\nu + \left|T_1\right|\right] & i > \left|T_1\right| \end{cases}$$

while the track distance relative to its associated tree row is given by

$$\upsilon(i) = \begin{cases} -\left(\mu + w\cdot\left[\left|T_1\right| - i^{*}\right]\right) & i \leq \left|T_1\right| \\ \mu + w\cdot\left[i^{*} - 1\right] & i > \left|T_1\right| \end{cases}$$

To estimate the distance between the relative positions of tracks *i* and *j*, the previous distance must be added to or subtracted from the distance of their corresponding tree rows. Consequently, the distance between any tracks $i, j \in T$ is given by

$$s(i,j) = \begin{cases} D_{\delta(i)\to\delta(j)} + \dfrac{\delta(i) - \delta(j)}{\left|\delta(i) - \delta(j)\right|}\left\{\upsilon(i) - \upsilon(j)\right\} & , \delta(i) \neq \delta(j) \\ \left|\upsilon(i) - \upsilon(j)\right| & , \delta(i) = \delta(j) \end{cases}$$

The cost for transitioning the machine between these two tracks is given again by $\Lambda\left(s(i,j)\right)$

2.3 THE ROBOTIC PLATFORM

For testing and validating purposes a deterministic behaviour field robot was implemented. The field robot AMS (autonomous mechanisation system) uses a modified conventional 20 kW tractor

(Hakotrac 3000, Hako-Werke GmbH, Bad Oldesloe, Germany) (Figure 4). The robot was built using the deterministic behaviour approach, wherein the mission (i.e., the route and the sequence of tasks) is planned in advance of the actual autonomous execution of the operation. The machine control system consists of a user interface that includes the mission definition, the high level control, and the low level control. It is based on the MobotWare system developed at Denmark's Technical University (Beck et al., 2010). The control system software for a task specific to a carried implement consists of a number of modules that include the projection of the GNSS measured position on the ground level, the filtering and temporal prediction of the position, the coordinate transformation of the implement reference point, the waypoint following, and the transverse and longitudinal control (depending on the operation) (Griepentrog et al., 2013).

The mission plan is defined in an XML formatted file (eXtendible Markup Language - IEEE Standard 1484.11.3-2005) (see next Section). The XML file is uploaded to the autonomous vehicle through the user interface. Mission files could be edited using an ASCII text file editor. A notebook computer communicates with the on-board robot computer through an Internet browser via a wireless local area network (WLAN). It is also used to display the graphical user interface for the navigation software and to upload the mission files.

Figure 4. The AMS field robot.

2.4 THE MISSION PLANNING SYSTEM

A complete mission plan for the autonomous vehicle was developed that includes the generation of the sequence of way-points, the actions that must be taken at each way point, and the operational status and the corresponding parameters while moving between subsequent way-points (Figure 5). The path is defined as a sequence of waypoints connected via either straight-line segments or predefined turning routine templates (e.g., Ω-turn and Tau-turn).

The first tags of the XML file relate to the mission initialisation. This includes defining the data to be logged in this mission (<log>) and how the Kalman filter should be initialised (<kalmaninit>). The latter is a standard path tracker that minimises the cross-track error in the connections between the waypoints. The waypoints are within the route tag described by a number of attributes that include its coordinates (in the Universal Transverse Mercator (UTM) coordinate system format), the speed and acceleration for driving to a particular waypoint from the preceding waypoint, and the actions that should be taken at that point, such as a potential stop at the waypoint (e.g. to adjust the carried implement), the raising or the lowering of the carried implement, the starting or stopping of the PTO (power take-off) shaft, and the predefined turning routine that should be executed (if a turn has to be performed) for connecting the current and the next route waypoint. Finally, the tag <field> provides the field polygon points that define the boundary within which the motion of the vehicle is restricted.

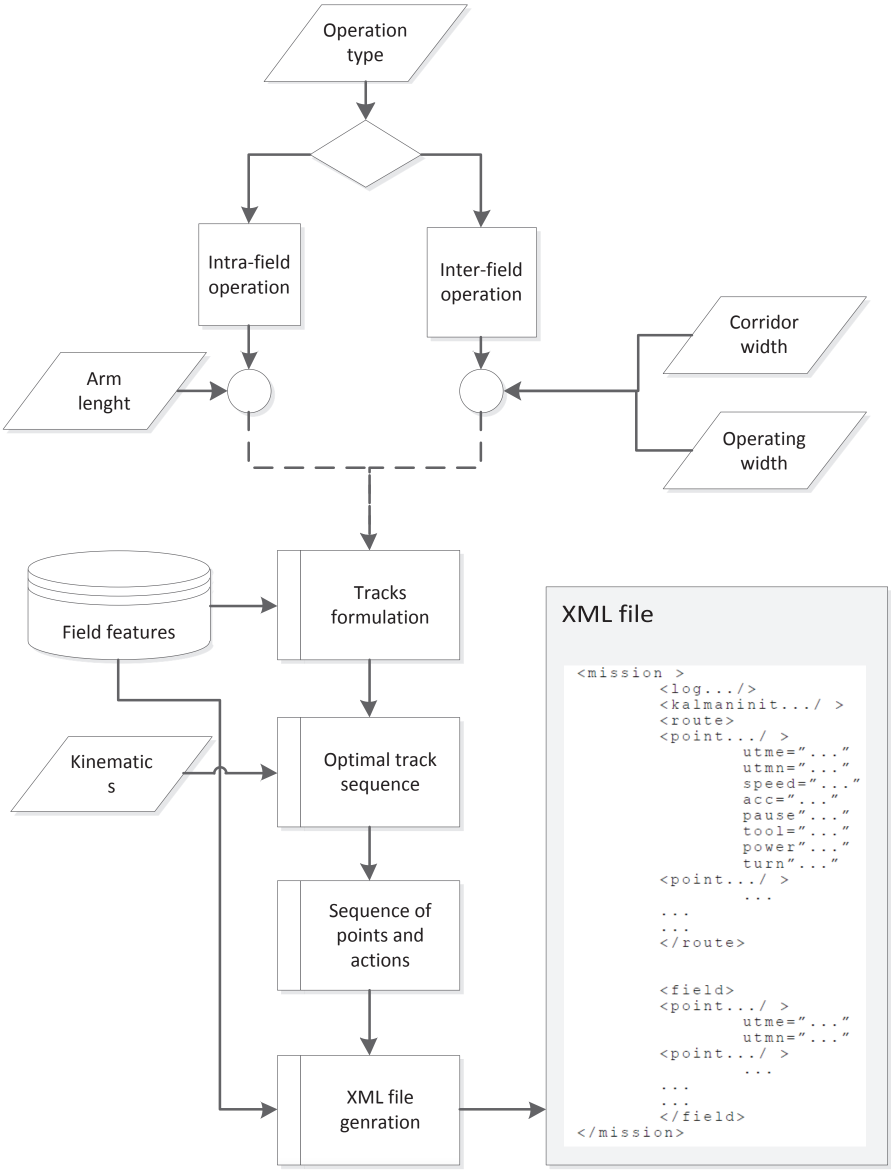

Figure 5. The mission planner architecture

3. EXPERIMENTAL RESULTS

A number of orchard operation examples were performed and are presented to demonstrate the above-mentioned route planning method and mission planning system. The experimental orchard is located the KU-LIFE Taastrup campus, Denmark [55° 40′ 08.57″ N, 12° 18′ 16.47″ E] and consists of 8 tree rows, each with an average length of 133.5 m and an inter-row distance equal to

5 m (Figure 6). For all of the executed operations, the entry and exit points were both located in the southeast corner of the orchard (the entry and exit nodes in the graph are coincident).

(a)

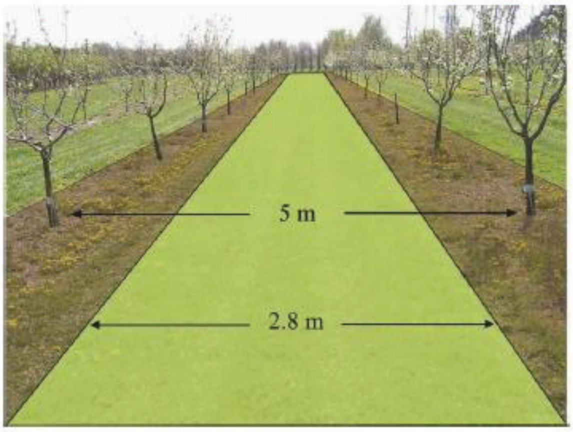

(b)

Figure 6. Part of the experimental orchard (a); the mowing area (green) and the weed spraying area (brown) (b).

The operations performed were a) grass cutting in the corridors and b) weed spraying a width of 1.1 m in each side of a row. All of the operations were executed twice, once by implementing the conventional track sequence, in which the vehicle follows a continuous pattern (i.e., the consecutive tracks covered by the machine are adjacent), and once by implementing the optimised track sequence (B-patterns) included in the mission planner. The comparison of the operational elements between the two cases (conventional vs. optimal) is presented in Table 1. Although the optimization criterion is the non-working travelled distance, a side effect of the reduction of the non-working distance is the reduction of the non-working operation time. Therefore, it seemed appropriate to include also time-specific results in Table 1. However, the non-working time is a relative measure of performance of the route planning method since it is dependent on the speed that headland turns are performed which varies between different vehicles, in the case of field robots, or different operators, in the case of conventional machines. Thus, the presented results on non-working time should be seen as indicative in terms of the potential savings of the route planning method since they are case depended in terms of the implemented vehicle.

3.1 WEED SPRAYING

A one-way oriented implement was adjusted on the right side of the autonomous tractor. The telescopic arm allowed for variable values of distance μ. Five weed spraying operations were performed using distances (μ) of 180 cm, 200 cm, 250 cm, 280 cm, and 300 cm. Selectively, the optimal planned operations for arm lengths of 300 and 200 cm are depicted in Figures 7a and 7b, respectively.

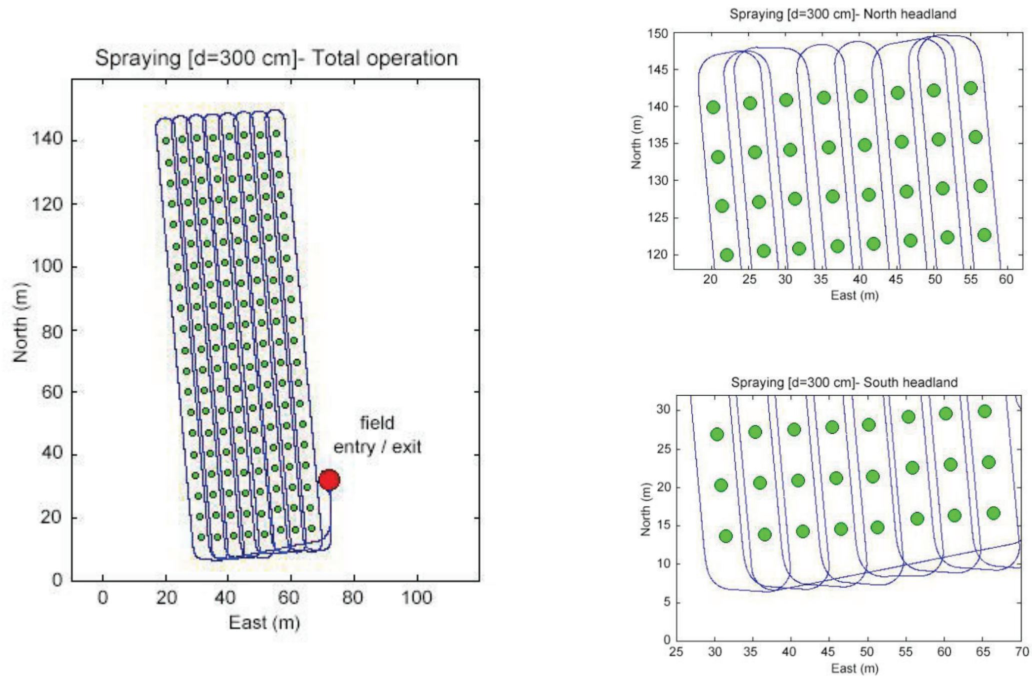

(a)

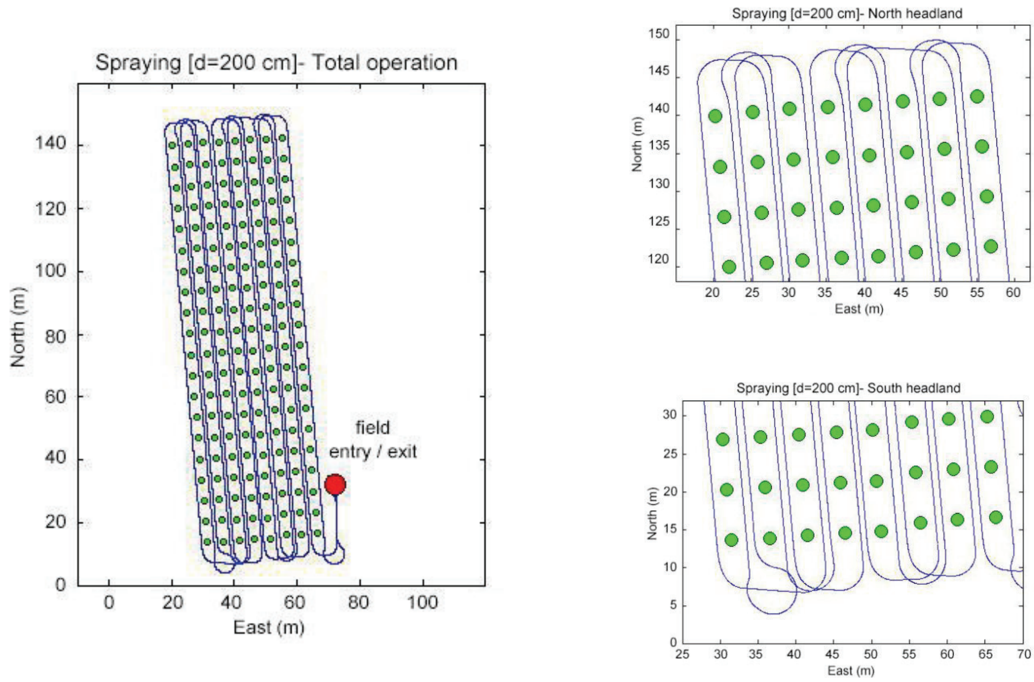

(b)

Figure 7. Intra-row weed spraying operation for arm distances (a) μ=300 cm and (b) μ=200 cm according to the optimal planning.

The track sequences for the optimal planning were as follows:

μ*=180 cm,* $\sigma^* =$<2 5 8 3 6 9 12 15 14 11 16 13 10 7 4 1>

μ*=200 cm,* $\sigma^* =$<2 5 8 3 6 9 12 15 14 11 16 13 10 7 4 1>

μ*=250 cm,* $\sigma^* =$<2 3 6 1 4 9 12 7 10 15 14 11 16 13 8 5>

μ*=280 cm,* $\sigma^* =$<2 3 6 7 10 15 14 11 16 13 12 9 8 5 4 1>

μ*=300 cm,* $\sigma^* =$<2 1 4 3 6 5 8 7 10 9 12 11 14 13 16 15>

During the spraying operation with the arm displacement at 300 cm, the numerical ordering of the generated tracks was not coincident with the spatial one. The spatial ordering of the tracks as they appear in Figurea, from left to right, is 1, 3, 2, 5, 4, and so on.

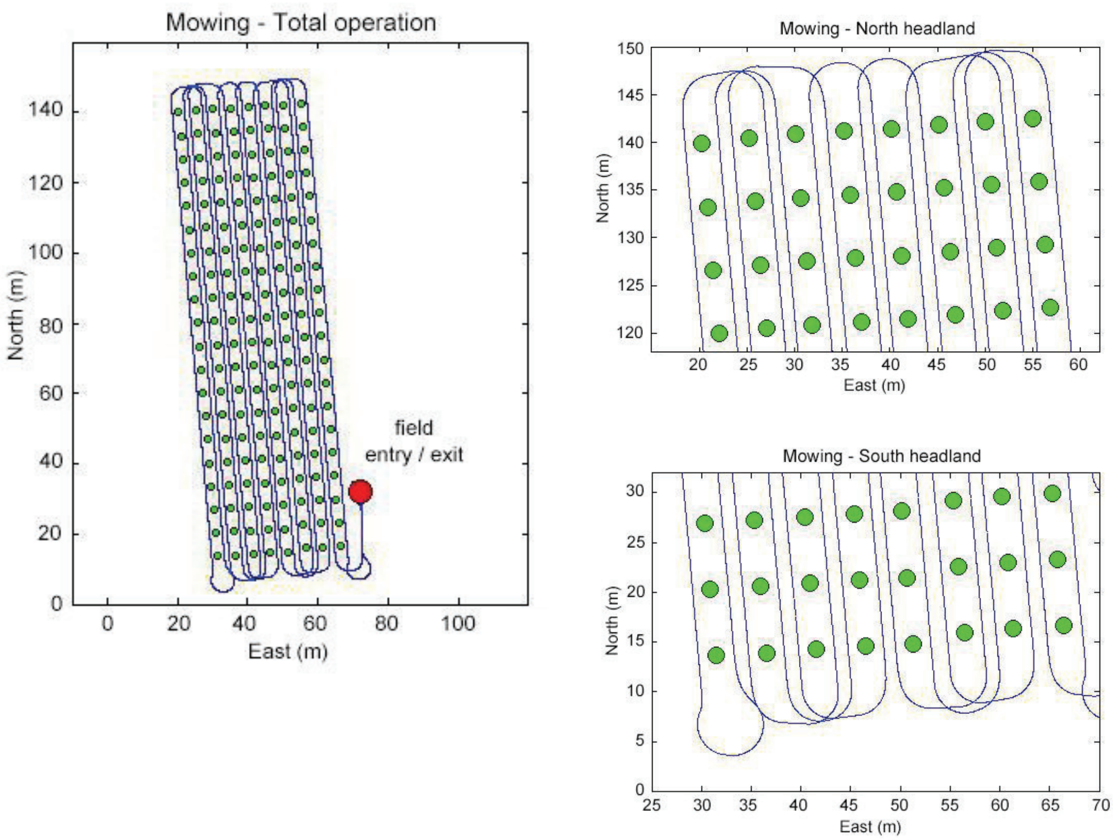

Figure 8 – Mowing operation according to the optimal planning.

3.2 MOWING OPERATION

The operating width of the mower was 1.4 m, and two passes in each inter-row corridor were required (app, 2.8 m). For this specific case, the number of the tracks in each sub-field was $|T_1| = |T_9| = 1, |T_i| = 2, i = 2,...,8$. The optimal track sequence was σ^*=<2 5 8 11 14 10 13 16 15 12 9 6 3 7 4 1> (Figure 8).

Table 1. Measured distance and time elements during experimental operations

		Distance				Time			
Operation	**Type**	**Total (m)**	**Savings# (%)**	**Non-working (m)**	**Savings# (%)**	**Total (s)**	**Savings# (%)**	**Non-working (s)**	**Savings# (%)**
Spraying μ=300 cm	B-patterns	2,393	2.2	257	17.5	2,893	2.5	628	10.7
	Conventional	2,447		312		2,968		703	
Spraying μ=280 cm	B-patterns	2,425	5.5	290	32.5	2,967	7.9	743	25.4
	Conventional	2,565		429		3,220		996	
Spraying μ=250 cm	B-patterns	2,466	3.3	331	20.1	3,064	5.9	871	18.0
	Conventional	2,549		414		3,256		1,063	
Spraying μ=200 cm	B-patterns	2,382	6.0	246	38.4	2,867	6.1	572	24.5
	Conventional	2,535		399		3,052		757	
Spraying μ=180 cm	B-patterns	2,362	6.3	226	41.1	2,821	8.6	555	32.4
	Conventional	2,520		384		3,087		821	
Mowing	B-patterns	2,374	6.4	239	40.2	2,850	8.6	597	31.0
	Conventional	2,535		399		3,119		866	

Depending on the element, distance or time, the savings was estimated as:

$$\frac{[\text{Value}]_{\text{Conventional}} - [\text{Value}]_{\text{B-pattern}}}{[\text{Value}]_{\text{Conventional}}} \cdot 100\%$$

3.3 SIMULATION EXPERIMENTS

In order to demonstrate the applicability of the approach in several orchard formats, e.g. polygonal, and orchards with curved rows, a number of simulated experiments were executed and presented. The simulations regard the cases of two virtual orchards formats, namely one polygonal-shaped orchard and one with curved tree rows. For each virtual orchard, two mowing operations were considered, one involving two passes in each inter-row corridor (inter-row distance: 5 m, operating width: 1.4 m) (Fig 9a and Fig 9b, for the polygonal and curved shape, respectively), and a second one involving three passes in each inter-row corridor (inter-row distance: 6 m, operating width: 1.2 m) (Fig 9c and Fig 9d, for the polygonal and curved shape, respectively), and one spraying operation (arm displacement at 200 cm) (Fig 9e and Fig 9f, for the polygonal and curved shape, respectively). A comparison between the optimized and conventional (track-by-track) routes, in terms of non-working travelled distance, for the simulated cases is given in Table 2.

Table 2. Comparison between the non-working distances travelled of the optimized and the conventional routes in the simulated experiments

	Case		**Total travelled distance (m)**	**Savings (%)**	**Non-working travelled distance (m)**	**Savings (%)**
Mowing	Polygon-shaped / 2 inter-row passes	B-patterns	786,8	8.2	161.5	30.4
		Conventional	857,2		231.9	
	Polygon-shaped / 3 inter-row passes	B-patterns	1187,4	8.4	255.4	30.0
		Conventional	1296,9		364.9	
	Curved-shaped / 2 inter-row passes	B-patterns	1013,1	9.3	138.4	43.0
		Conventional	1117,5		242.8	
	Curved-shaped / 3 inter-row passes	B-patterns	1522,2	8.7	227.2	39.1
		Conventional	1667,8		372.8	
Spraying	Polygon-shaped	B-patterns	798,2	6.4	170.2	24.4
		Conventional	853,2		225.2	
	Curved-shaped	B-patterns	1063,7	5.1	176.9	24.3
		Conventional	1120,6		233.8	

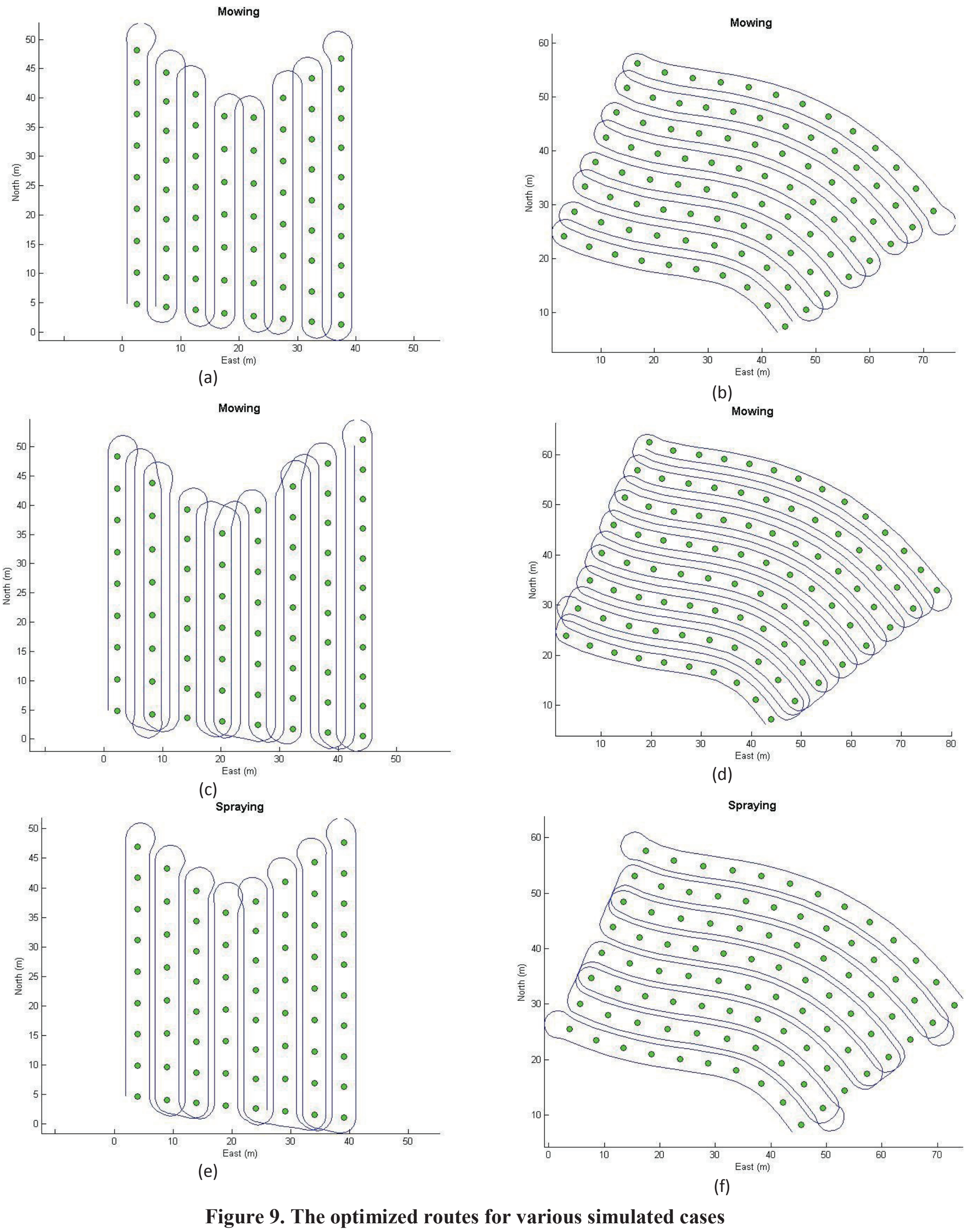

Figure 9. The optimized routes for various simulated cases

4. DISCUSSION

The presented route planning approach is an adaptation of the B-pattern method in the sense that it provides a framework to encode orchard operations into the TSP cost matrix. For the implementation of the route planning the position of every tree is not really needed. The GPS positions of two trees at the "lower" and "upper" edge of a tree-row are needed to form matrices $\mathbf{U_R}$ and $\mathbf{U_L}$. As long as he two geo-referenced points that define the upper and lower end of each row can be found, the methodology can be used. In this paper known GPS coordinates were used. In another scenario, these points could be extracted from georeferenced aerial images; the same is true for row heading angle. In practical situations (curved or nonlinear or crooked rows), the two end-points of each row should be fed to the robot but reactive navigation will be necessary.

In the experimental operations, the Ω-turn was executed in the cases for which the robot's kinematic restriction ($2r_{\min} > s(i, j)$) did not allow for the execution of a Π-turn. This was based on the fact that in this specific orchard, there was sufficient space in the headlands areas for the execution of Ω-turns. If this were not the case, the robot would be restricted to executing a Tau-turn instead of a Ω-turn because of the reduced required space for manoeuvring (identical to that required in the case of a Π-turn). However, the optimal sequence would be identical because for this specific robot, the turning time for a Tau-turn is similar to that required to execute an Ω-turn between the same initial and final track.

As listed in Table 1, in the case in which the μ distance was adjusted to 250 cm, the non-working distance during turning was measured to be 312 m, whereas in the case in which the μ distance was adjusted to 180 cm, the non-working distance was 216 m. It can be observed that different adjustments of distance μ can result in a relative decrease of up to 31% of the non-working distance when comparing the optimal solutions for both cases. This decrease in the non-working distance translates to a greater decrease (when comparing the optimal solutions for both cases) in the total operational time (in this specific case, 3.2%). However, the specific experimental orchard has a shape that can provide high field efficiency specific to the orchard shape (long length-short width rectangular). In cases in which the turning time is a considerable part of the total operational time, the reduction is considerably higher. This provides the opportunity for an offline estimation of the non-working travelled distance for various values of the parameter μ and for the selection of an optimal one for the specific orchard and the specific kinematics that apply to the agricultural vehicle performing the operation.

5. Conclusions

A route planning approach for orchard operations has been developed and validated. At its core, the planning method has the generation of optimal route planning based on the adaptation of the B-patterns area coverage approach developed for arable farming operations. The resulting operation plans are optimal when using the non-working travelled distance as the criterion. Experiments have verified that the operational efficiency can be improved significantly over that of the conventional non-optimised method of executing orchard operations using conventional machines. Specifically, as shown by the experimental results, the reduction in the non-working time ranged between 10.7% and 32.4%, and the reduction in the non-working distance ranged between 17.5% and 40.2%, resulting to savings in the total travelled distance ranged between 2.2% and 6.4%. The next steps for this planning method relate to its expansion to autonomous orchard operations constrained by the carrying capacity of the machine (e.g., spraying operations) and to multiple neighbouring orchard operations. This further research will provide a complete route planning system for autonomous orchard vehicles. .

References

Barawid Jr, O.C., Mizushima, A., Ishii, K., Noguchi, N. (2007). Development of an Autonomous Navigation System using a Two-dimensional Laser Scanner in an Orchard Application.

Beck, A.B., Andersen, N.A, Andersen, J.C., & Ravn, O. (2010). MobotWare—a plug-in based framework for mobile robots. In: Proceedings IFAC symposium on intelligent autonomous vehicles, July 2010, Lecce, Italy, International Federation of Automatic Control (IFAC)

Bochtis, D. D. (2008). Planning and control of a fleet of agricultural machines for optimal management of field operations. Greece: Aristotle University. Ph.D. Thesis.

Bochtis, D.D.,& Vougioukas, S.G. (2008). Minimising the non-working distance travelled by machines operating in a headland field pattern. Biosystems Engineering, 101(1), 1–12.

Bochtis, D. D., & Sørensen, C. G. (2009). The vehicle routing problem in field logistics: part I. Biosystems Engineering, 104(4), 447-457.

Bochtis, D. D., Vougioukas, S. G., & Griepentrog, H. W. (2009). A mission planner for an autonomous tractor. Transactions of the ASABE, 52, 1429-1440.

Bochtis, D.D., Sørensen, C.G., Busato, P., & Berruto R. (2013). Benefits from optimal route planning based on *B-patterns*. Biosystems Engineering, 115, 389-395.

De-An, Z., Jidong, L., Wei, Z., Ying, Z., & Yu, C. (2011). Design and control of an apple harvesting robot. Biosystems Engineering, 110, 112-122.

Ferguson, D., Stentz, A. (2006). Using interpolation to improve path planning: the field D* algorithm. Journal of Field Robotics, 23, 79–101.

Griepentrog, H.W., Dühring Jaeger, C.L., & Paraforos D.S. (2013). Robots for Field Operations with Comprehensive Multilayer Control. Künstl Intell, 27,325–333.

Heidman, B.C., Rosa, U. A. (2008). Real-Time Tree Localization in Orchards. Applied Engineering in Agriculture. 24(6): 707-716.

Hiremath, S.A., van der Heijden, G.W.A.M., van Evert, F.K., Stein, A., ter Braak, C.J.F. 2014b. Laser range finder model for autonomous navigation of a robot in a maize field using a particle filter, Computers and Electronics in Agriculture, 100, 41-50.

Kise, M., Zhang, Q., Rovira Mas, F. (2005). A stereovision-based crop row detection method for tractor-automated guidance. Biosystems Engineering, 90(4), 357–367

Linker, R., & Blass, T. (2008). Path-planning algorithm for vehicles operating in orchards. Biosystens Engineering, 101, 152-160.

Rovira-Mas F; Zhang Q; Reid J F; Will J D (2005). Houghtransform-based vision algorithm for crop row detection of an automated agricultural vehicle. Journal of Automobile Engineering, 219(8), 999–1010.

Subramanian, V., Burks, T.F., Arroyo, A.A. (2006). Development of machine vision and laser radar based autonomous vehicle guidance systems for citrus grove navigation. Computers and Electronics in Agriculture, 53, 130-143.

Subramanian, V. , Burks, T. F., Dixon W. E. (2009). Sensor Fusion Using Fuzzy Logic Enhanced Kalman Filter for Autonomous Vehicle Guidance in Citrus Groves. Transactions of the ASABE. 52(5): 1411-1422.

Tanigaki, K., Fujiura, T., Akase, A., & Imagawa, J. (2008). Cherry-harvesting robot. Computers and Electronics in Agriculture, 63, 65-72.

Tosaki, K., Miyahara, S., Ichikawa, T., & Mizukura,Y. (1996). Development of Microcomputer Controlled Driverless Air Blast Sprayer (Part 1). Journal of JSAM, 58(6), 101-110.

Tsubota, R., Noguchi, N., & Mizushima, A. (2004). Automatic guidance with a laser scanner for a robot tractor in an orchard. In Proceedings Automation Technology for Off-Road Equipment, 7-8 October 2004, Kyoto, Japan, ASAE Publication Number 701P1004. Eds. Q. Zhang, M. Iida, A. Mizushima.

Yekutieli, O., Pegna, F.G., 2002. Automatic guidance of a tractor in a vineyard. In: Proceedings of the Automation Technology for Off-road Equipment, Illinois, USA.

Table

Table 1. Measured distance and time elements during experimental operations

		Distance				Time			
Operation	**Type**	**Total (m)**	**Savings# (%)**	**Non-working (m)**	**Savings# (%)**	**Total (s)**	**Savings# (%)**	**Non-working (s)**	**Savings# (%)**
Spraying *μ*=300 cm	B-patterns	2,393	2.2	257	17.5	2,893	2.5	628	10.7
	Conventional	2,447		312		2,968		703	
Spraying *μ*=280 cm	B-patterns	2,425	5.5	290	32.5	2,967	7.9	743	25.4
	Conventional	2,565		429		3,220		996	
Spraying *μ*=250 cm	B-patterns	2,466	3.3	331	20.1	3,064	5.9	871	18.0
	Conventional	2,549		414		3,256		1,063	
Spraying *μ*=200 cm	B-patterns	2,382	6.0	246	38.4	2,867	6.1	572	24.5
	Conventional	2,535		399		3,052		757	
Spraying *μ*=180 cm	B-patterns	2,362	6.3	226	41.1	2,821	8.6	555	32.4
	Conventional	2,520		384		3,087		821	
Mowing	B-patterns	2,374	6.4	239	40.2	2,850	8.6	597	31.0
	Conventional	2,535		399		3,119		866	

Depending on the element, distance or time, the savings was estimated as:

$$\frac{[\text{Value}]_{\text{Conventional}} - [\text{Value}]_{\text{B-pattern}}}{[\text{Value}]_{\text{Conventional}}} \cdot 100\%$$

Table

Table 2. Comparison between the non-working distances travelled of the optimized and the conventional routes in the simulated experiments

	Case		**Total travelled distance (m)**	**Savings (%)**	**Non-working travelled distance (m)**	**Savings (%)**
Mowing	Polygon-shaped / 2 inter-row passes	B-patterns	786,8	8.2	161.5	30.4
		Conventional	857,2		231.9	
	Polygon-shaped / 3 inter-row passes	B-patterns	1187,4	8.4	255.4	30.0
		Conventional	1296,9		364.9	
	Curved-shaped / 2 inter-row passes	B-patterns	1013,1	9.3	138.4	43.0
		Conventional	1117,5		242.8	
	Curved-shaped / 3 inter-row passes	B-patterns	1522,2	8.7	227.2	39.1
		Conventional	1667,8		372.8	
Spraying	Polygon-shaped	B-patterns	798,2	6.4	170.2	24.4
		Conventional	853,2		225.2	
	Curved-shaped	B-patterns	1063,7	5.1	176.9	24.3
		Conventional	1120,6		233.8	

Figure
Click here to download Figure: Figure 1.docx

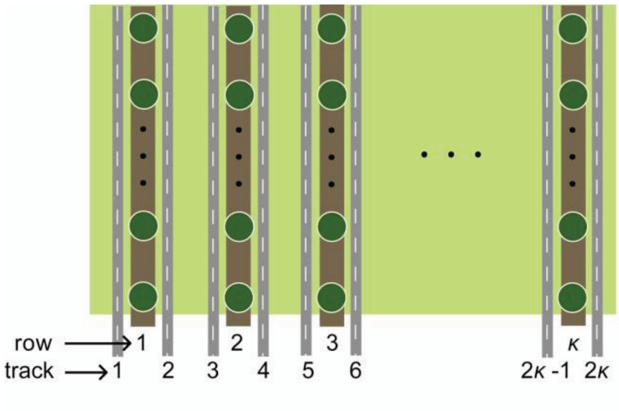

Figure 1. The derived tracks for intra-row orchard operations.

Figure

Click here to download Figure: Figure 2.docx

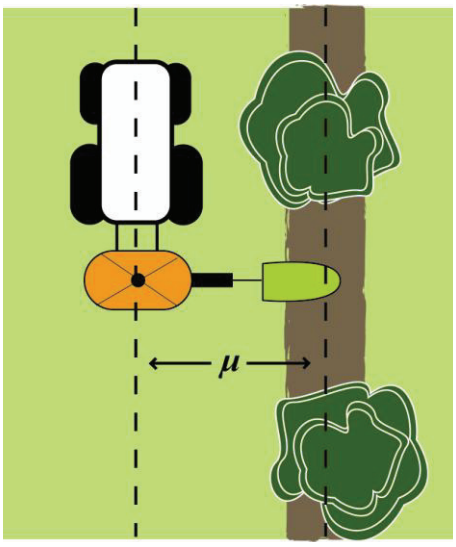

Figure 2. Vehicle positioning in intra-row operations

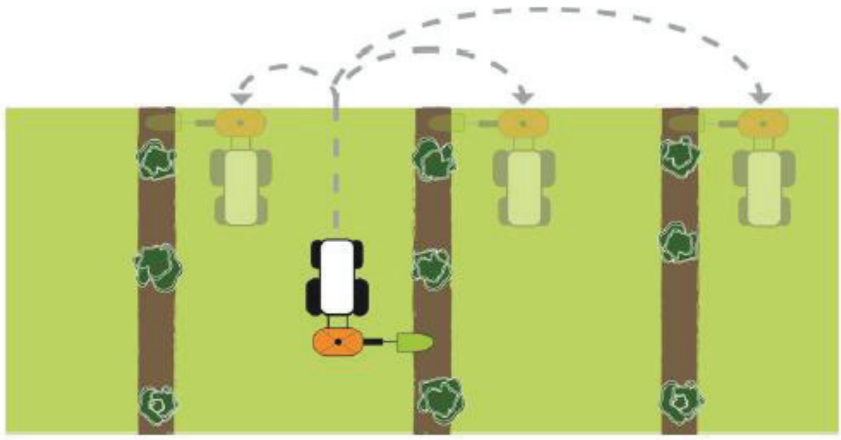

(a)

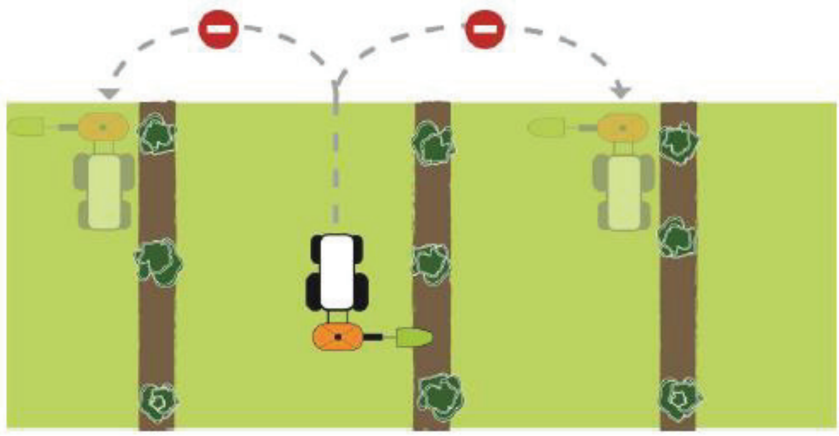

(b)

Figure 3 – Disallowed transitions for a robot carrying a one-way oriented implement.

Figure
Click here to download Figure: Figure 4.docx

Figure 4. The AMS field robot.

Figure
Click here to download Figure: Figure 5.docx

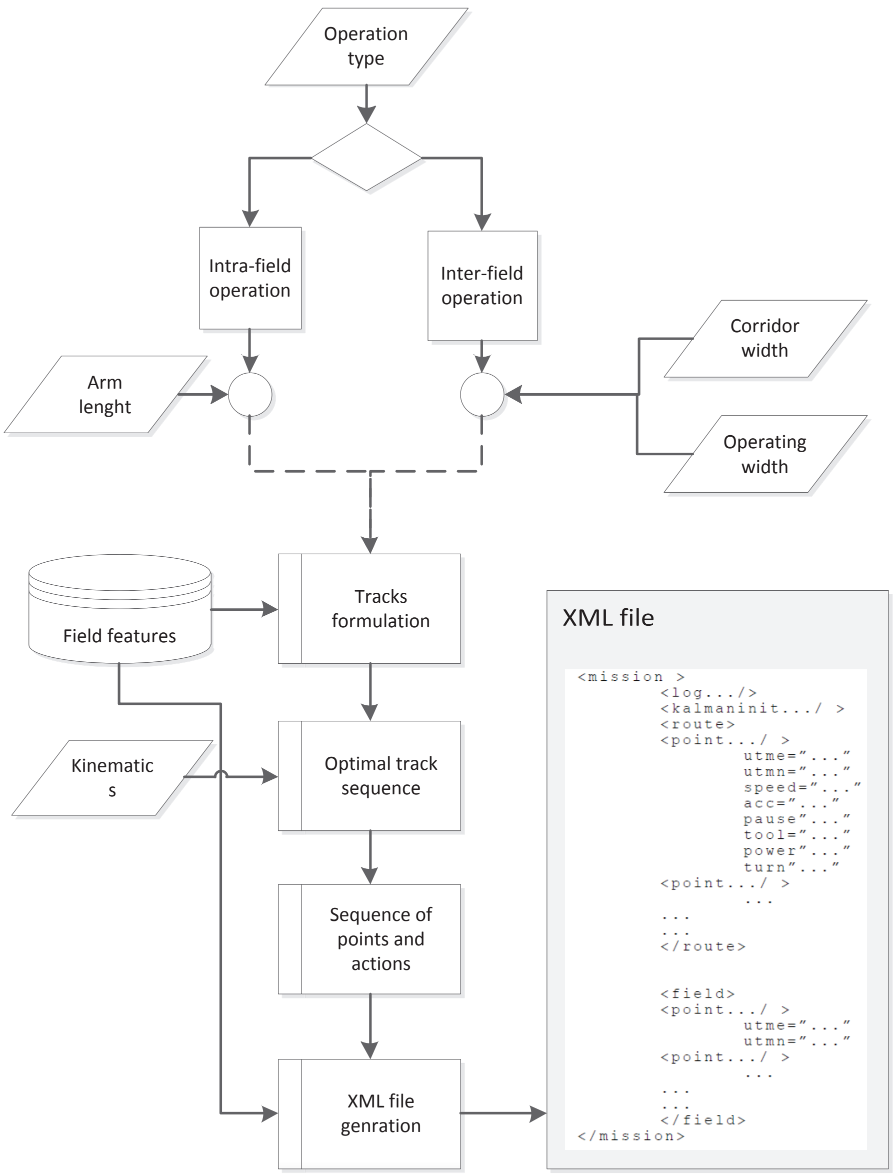

Figure 5. The mission planner architecture

Figure
Click here to download Figure: Figure 6.docx

(a)

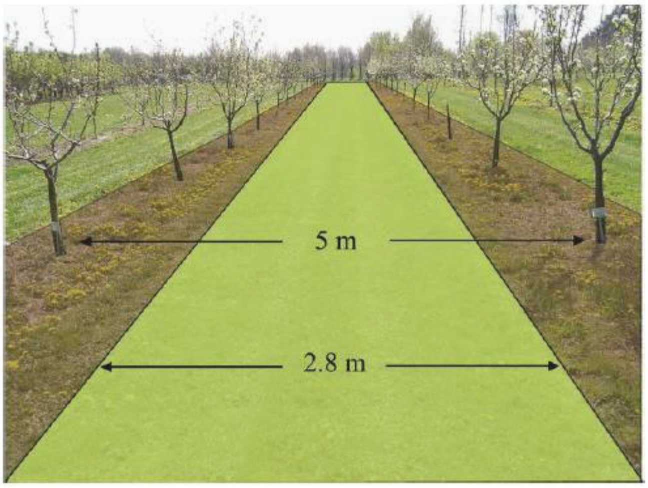

(b)

Figure 6. Part of the experimental orchard (a); the mowing area (green) and the weed spraying area (brown) (b).

Figure

Click here to download Figure: Figure 7 REVISED.docx

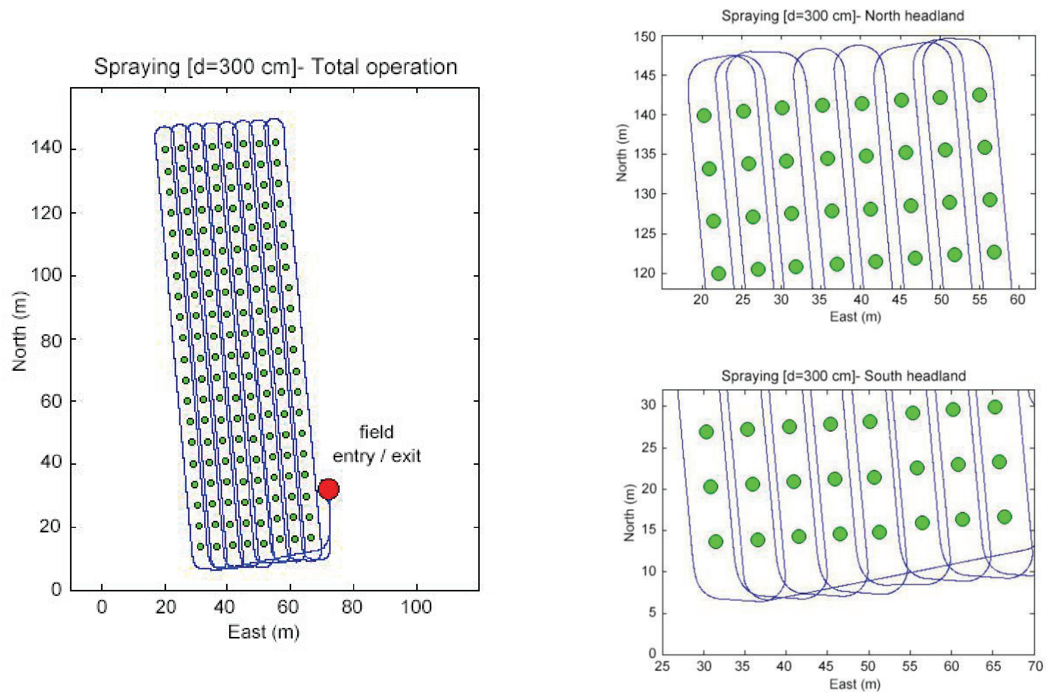

(a)

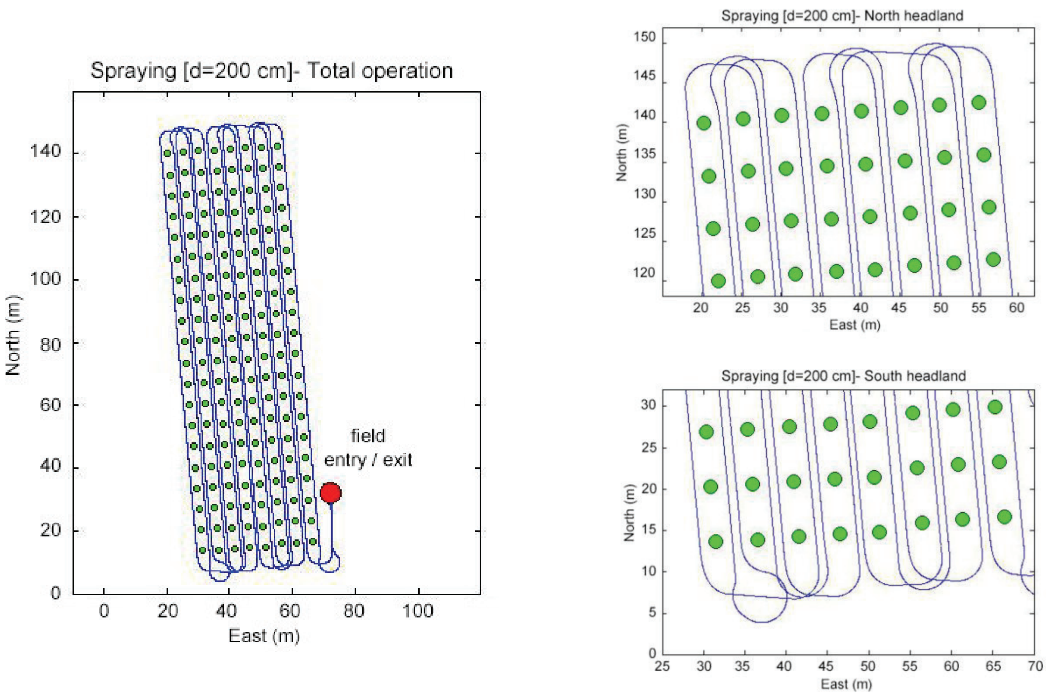

(b)

Figure 7. Intra-row weed spraying operation for arm distances (a) μ=300 cm and (b) μ=200 cm according to the optimal planning.

Figure
Click here to download Figure: Figure 8 REVISED.docx

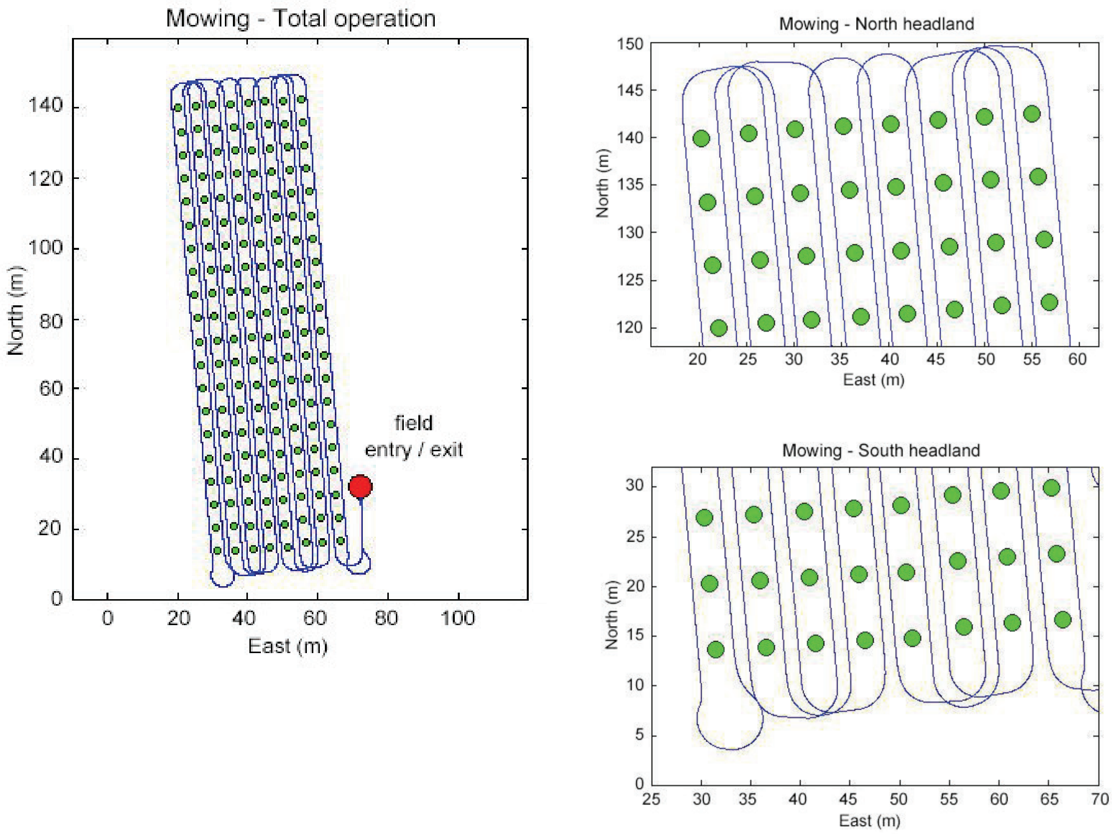

Figure 8 – Mowing operation according to the optimal planning.

Figure

Click here to download Figure: Figure 9.docx

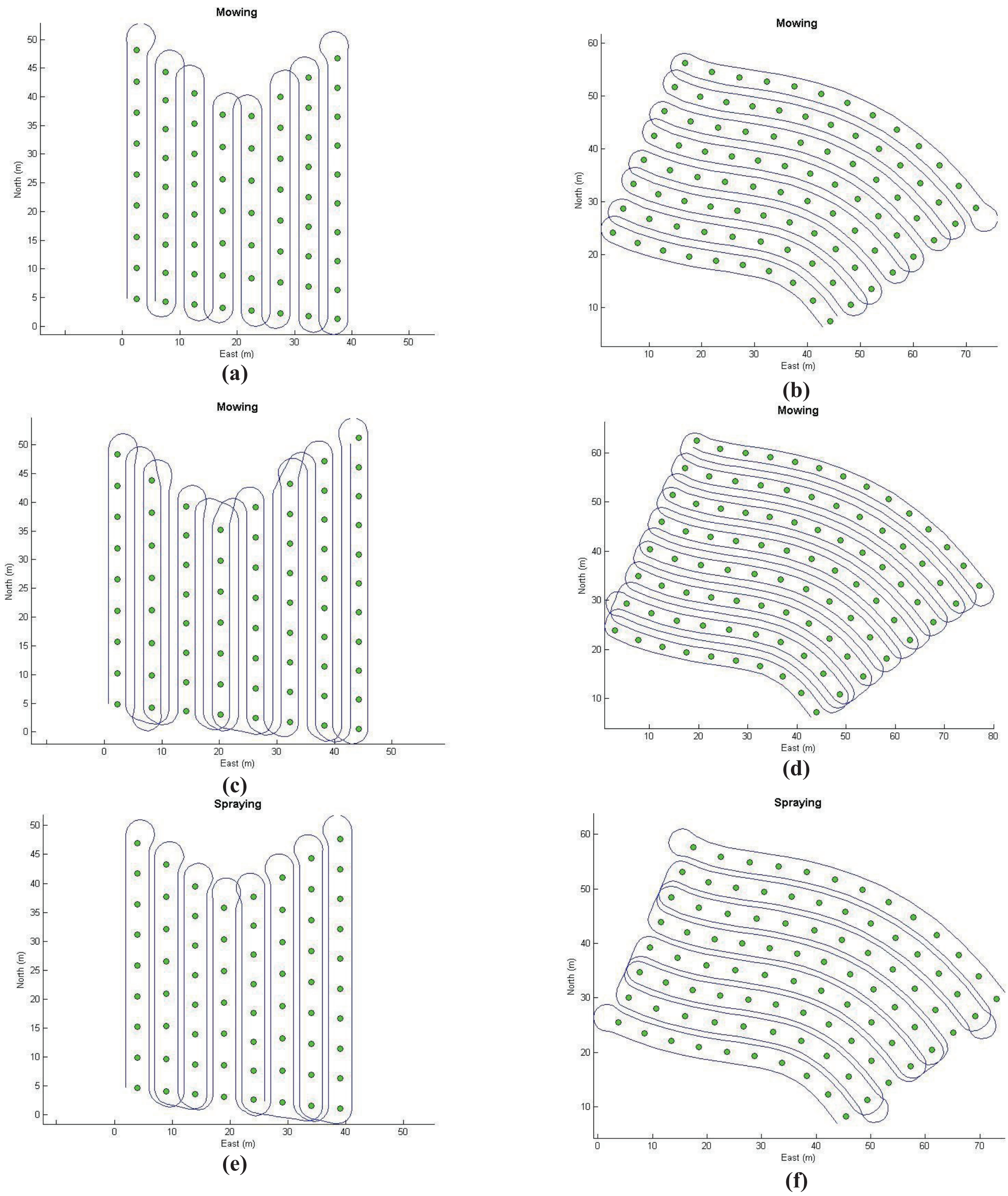

Figure 9. The optimized routes for various simulated cases